Naval Research Laboratory
Washington, DC 20375-5000

NRL Memorandum Report 6872

Multimode Simulation of High Frequency Gyrotrons

S. H. GOLD AND A. W. FLIFLET

Beam Physics Branch
Plasma Physics Division

September 5, 1991

REPORT DOCUMENTATION PAGE

Form Approved
OMB No 0704-0188

1. AGENCY USE ONLY (Leave blank)	2. REPORT DATE	3. REPORT TYPE AND DATES COVERED
	1991 September 5	Interim

4. TITLE AND SUBTITLE

Multimode Simulation of High Frequency Gyrotrons

5. FUNDING NUMBERS

JO# 47-2797-0-1

6. AUTHOR(S)

S. H. Gold and A. W. Fliflet

7. PERFORMING ORGANIZATION NAME(S) AND ADDRESS(ES)

Naval Research Laboratory
Washington, DC 20375-5000

8. PERFORMING ORGANIZATION REPORT NUMBER

NRL Memorandum Report 6872

9. SPONSORING/MONITORING AGENCY NAME(S) AND ADDRESS(ES)

U. S. Department of Energy
Washington, DC 20545

10. SPONSORING/MONITORING AGENCY REPORT NUMBER

11. SUPPLEMENTARY NOTES

12a. DISTRIBUTION/AVAILABILITY STATEMENT

Approved for public release, distribution is unlimited

12b. DISTRIBUTION CODE

13. ABSTRACT (Maximum 200 words)

This paper presents a simulation study of mode competition in highly overmoded gyrotron cavities. The parameters of the study have been selected to correspond to the approximate design parameters of a 280 GHz, 1 MW gyrotron at the Massachusetts Institute of Technology (MIT). The MIT gyrotron is designed to run in the $TE_{+42,7}$ mode. using a 50 A, 84 keV electron beam, with a normalized beam radius of 0.6, and a beam α of 1.6. This study addresses 1) the problem of achieving gyrotron operation in the design mode, and at a value of magnetic detuning sufficient to achieve high efficiency operation, and 2) the mode purity of the final state.

14. SUBJECT TERMS

Gyrotron
Mode competition
Numerical Simulation

15. NUMBER OF PAGES

32

16. PRICE CODE

17. SECURITY CLASSIFICATION OF REPORT	18. SECURITY CLASSIFICATION OF THIS PAGE	19. SECURITY CLASSIFICATION OF ABSTRACT	20. LIMITATION OF ABSTRACT
UNCLASSIFIED	UNCLASSIFIED	UNCLASSIFIED	SAR

CONTENTS

MULTIMODE SIMULATION OF HIGH FREQUENCY GYROTRONS

I. Introduction

The effort to push gyrotron oscillators to ever higher frequencies and power levels has led to the employment of ever higher order transverse cavity modes. Maximum gyrotron efficiency is generally achieved by optimizing the magnetic detuning for a single mode. This becomes progressively more difficult to do as the fractional mode spacing shrinks, since 1) the intended mode may never start oscillation, or 2) it may be unstable at its optimum detuning in the presence of competition from nearby modes, or 3) the final state may be a multimode state. In this paper, we use a time–dependent multimode simulation code (Fliflet *et al.* 1991) to examine the optimization of the gyrotron parameters for the 280 GHz $TE_{42,7}$–mode gyrotron experiment being set up by Kreischer and coworkers at the Massachusetts Institute of Technology (MIT), in the presence of competition from nearby $TE_{m,7}$ and other $TE_{m,\ell}$ modes.

A classical multimode theory of lasers was obtained by Lamb (1964) and Sargent *et al.* (1974). The full nonlinear system of coupled equations for the interacting modes was simplified by means of a perturbation expansion in powers of the electric field amplitudes. This theory was adapted to the multimode operation of gyrotrons by Nusinovich and co–workers (Moiseev and Nusinovich 1974, Nusinovich 1981) who also made use of a perturbation expansion in the mode amplitudes. A fully nonlinear, time–dependent multimode theory of quasi–optical gyrotrons has been developed by Bondeson *et al* (1983). The stability of single–mode gyrotron operation with respect to parasitic oscillations has been examined by Antonsen *et al.* (1990), Levush and Antonsen (1991), Dumbrajs *et al.* (1988), and Borie and Jödicke (1988). Multimode effects in gyrotron have also been studied using a particle–in–cell (PIC) code by Lin and co–workers (Lin *et al.* 1988). The theoretical basis for the present

Manuscript approved June 13, 1991.

calculations is developed in Fliflet *et al.* (1991). A fully nonlinear formulation is desirable when the operating current is many times higher than the threshold current. As discussed below, there is a difficulty in nonlinear multimode calculations for configurations involving several modes with different azimuthal and radial mode indices. This difficulty is associated with the large number of initial phases needed to average over the possible relative initial phases of the interacting modes which in some cases can increase the multimode computation time by a factor of 100–1000 over a corresponding single mode calculation. Such calculations have recently become feasible given adequate access to a fast computer such as the Cray.

In this paper, a time–dependent multimode simulation code was used as a tool to study the overall mode competition problem, including competition between co– and counterrotating $TE_{\pm m,\ell}$ modes for the same m and ℓ, between members of a series of $TE_{m,\ell}$ modes with the same value of ℓ, and between $TE_{m,\ell}$ modes with different values of m and ℓ. Here, the azimuthal mode index, m, is generally assumed to take both positive and negative integral values. However, for the sake of clarity, when either $+m$ or $-m$ is explicitly used, it is assumed that m is a positive integer. The use of the plus (minus) sign in the azimuthal mode index, for a particular $TE_{\pm m,\ell}$ mode, refers to the sense of rotation of the mode, corresponding to co– (counter–) rotation of the mode with respect to the sense of electron gyration in the applied axial magnetic field.

II. Outline of Theory

The total transverse electric field in the gyrotron resonator is expanded in a series of transverse modes as follows:

$$\vec{E} = \sum_{n=1}^{N} a_n(z)\hat{n}(z)\vec{e}_n(r,\theta;z)e^{-i(\omega_0 t+\psi_n(z))} \qquad (1)$$

where $a_n(t)$ is the time dependent mode amplitude, $h(z)$ is the axial profile function, $\vec{e}_n$ is the mode transverse vector function, ω_0 is the reference wave frequency, and ψ_n is a slow–time–scale mode phase parameter. The free–running oscillator equations for the mode amplitude and phase, are given by:

$$\frac{da_n}{dt} + \frac{\omega_0 a_n}{2Q_n} = \frac{\omega_0}{2\varepsilon_0} \operatorname{Im} P_n(t) \tag{2}$$

$$\frac{d\psi_n}{dt} + \omega_0 = \omega_{n0} - \frac{\omega_0}{2\varepsilon_0 a_n} \operatorname{Re} P_n(t) \tag{3}$$

where

$$P_n(t) = \frac{i}{W} \frac{1}{2\pi} \int_0^{2\pi} d(\omega_0 t) \int_V d^3r\, h(z) \vec{e}^{\,*}_n \cdot \vec{J}_t\, e^{i(\omega_0 t + \psi_n)} \tag{4}$$

is the complex, slow–time–scale component of the electron beam polarization for the mode n, $W = \int_0^L dz |h(z)|^2$, ω_{n0} is the cold cavity eigenfrequency (taken to be positive for both co– and counterrotating modes), and ε_0 is the free space permittivity. To calculate the ac current density, the interaction with the electron beam is treated in the single–particle approximation. The general time–dependent problem can be simplified by using the fact that the characteristic risetime of fields in the resonator is much longer than the electron transit time in the cavity as well as the wave period. In this case, one can use a quasi–steady–state approximation, in which the electron trajectories are calculated for rf modes with fixed amplitude and linearized phase.

The slow–time–scale nonlinear equations of motion for an electron in a thin annular beam immersed in a tapered magnetic field and interacting at a particular harmonic with several circularly–polarized TE modes have been given previously by Fliflet (1986) and Fliflet *et al.* (1982), and are given by:

$$\frac{du_t}{d\bar{z}} = -\frac{\gamma}{u_z} \sum_{n=1}^{N} f_n J_s'(\bar{k}_t \bar{r}_L) \operatorname{Re}\left\{ \left(h + i \frac{u_z}{\gamma \bar{\omega}_0} \frac{dh}{d\bar{z}} \right) e^{-i\left[\Lambda + \tilde{\psi}_n + (m_n - m_r)\Theta_0\right]} \right\}$$
$$+ \frac{u_t}{2\bar{\Omega}_z} \frac{d\bar{\Omega}_z}{d\bar{z}} \tag{5}$$

$$\frac{d\Lambda}{d\bar{z}} = \bar{\omega}_0\left(1-\frac{s\bar{\Omega}\gamma_0}{\bar{\omega}_0\gamma}\right)$$
$$-\frac{s\gamma}{u_z u_t}\sum_{n=1}^{N} f_n \frac{sJ_s'(\bar{k}_t\bar{r}_L)}{\bar{k}_t\bar{r}_L}\,\mathrm{Re}\left\{\left(h+i\frac{u_z}{\gamma\bar{\omega}_0}\frac{dh}{d\bar{z}}-\frac{\bar{\omega}_{n0}^2\,u_t^2}{s\Omega\bar{\omega}_0\,\gamma}h\right)e^{-i\left[\Lambda+\tilde{\psi}_n+(m_n-m_\tau)\Theta_0\right]}\right\} \quad (6)$$

$$\frac{du_z}{d\bar{z}} = \frac{u_t}{u_z\bar{\omega}_0}\sum_{n=1}^{N} f_n J_s'(\bar{k}_t\bar{r}_L)\,\mathrm{Re}\left\{i\frac{dh}{d\bar{z}}e^{-i\left[\Lambda+\tilde{\psi}_n+(m_n-m_\tau)\Theta_0\right]}\right\}-\frac{u_t^2}{2u_z\bar{\Omega}_z}\frac{d\bar{\Omega}_z}{d\bar{z}} \quad (7)$$

where $u_t = \gamma v_t / c$ is the normalized transverse momentum amplitude, $u_z = \gamma v_z / c$ is the normalized axial momentum (v_t and v_z denote the electron transverse and axial velocities, respectively),

$$\Lambda = \left(\bar{\omega}_0 - s\bar{\Omega}/\gamma_0\right)\bar{z}/\beta_z + \omega_0 t_{0i} - s\phi - (m_\tau - s)\Theta_0 \quad (8)$$

gives the slow variation in the transverse momentum azimuthal phase relative to the reference wave phase,

$$\tilde{\psi}_n = \psi_n(\tau_0) + \left.\frac{d\psi_n}{d\tau}\right|_{\tau_0}\frac{\bar{\omega}_0}{\beta_{z0}}\bar{z} \quad (9)$$

is a phase correction corresponding to the difference between the mode frequency and the reference frequency, m_τ is the azimuthal index of a particular mode called the reference mode, $\beta_z = v_z / c$, and $\tau = \omega_0 t$. Other parameters include s, the harmonic number, γ (γ_0), the (initial) relativistic mass ratio which is given by:

$$\gamma = \left(1+u_t^2+u_z^2\right)^{1/2}, \quad (10)$$

k_t, the mode transverse wave number, r_L, the Larmor radius of the orbit, J_s(J_s'), the (derivative of) a regular Bessel function, Ω_z, the nonrelativistic cyclotron frequency for the z–component of the magnetic field, Ω, the value of Ω_z at the resonator entrance, t_{0i}, the time the electron enters the cavity, and f_n, the normalized mode amplitude with azimuthal dependence $e^{im_n\theta}$. The mode amplitude for $m_n > 0$ is normalized according to:

$$f_n = \frac{|e|}{mc^2} x'_n C_n J_{m_n - s}(k_{nt} R_0) a_n(t_0) \tag{11}$$

The sign of m_n determines the direction of mode rotation, as discussed previously. The normalized wave amplitude for $m_n < 0$ is given by Eq. (11), with m_n replaced by $|m_n|$ and $J_{m_n - s}(k_{nt} R_0)$ replaced by $(-1)^s J_{|m_n|+s}(k_{nt} R_0)$. Quantities with an overbar have been normalized according to: $\bar{z} = z / r_w$, $\bar{r}_L = r_L / r_w$, $\overline{\Omega} = \Omega r_w / c$, $\overline{\omega}_0 = \omega_0 r_w / c$, and $\bar{k}_{nt} = k_{nt} r_w$. R_0 and Θ_0 denote the electron orbit guiding center radius and azimuthal angle, $|e|$ is the electron charge, m_0 is the electron rest mass, m_n is the azimuthal index for the mode n, $x'_n = x'_{m_n \ell_n}$ is a zero of J_m', ℓ_n is the radial mode index, r_w is an arbitrary normalization radius, and ϕ gives the slow variation in the transverse momentum phase relative to the cyclotron motion. The transverse TE–mode normalization coefficient is given by:

$$C_n = \left\{ \left[\pi \left(x'^2_{m_n \ell_n} - m_n^2 \right) \right]^{1/2} J_{m_n}\left(x'_{m_n \ell_n} \right) \right\}^{-1} \tag{12}$$

The ac current density is obtained by integrating Eqs.(5)–(7) for an appropriate set of initial conditions at the cavity input, z=0. For a thin annular beam, the transverse ac current density is given by:

$$\vec{J}_t = -\frac{I_0}{v_z} \vec{v}_t \tag{13}$$

Using the prescription developed in previously in Fliflet *et al.* (1991), the mode amplitude and phase can be rewritten as:

$$\frac{df_n}{d\tau} = -\frac{f_n}{2Q_n} + \tilde{I}_n \int_0^{\bar{L}} d\bar{z}\, h(\bar{z}) \left\langle J'_s(k_{nt} r_L) \frac{u_t}{u_z} \cos\left[\Lambda + \tilde{\psi}_n - (m_n - m_\tau)\Theta_0 \right] \right\rangle_{\Lambda_0, \Theta_0} \tag{14}$$

$$\frac{d\psi_n}{d\tau} = -\frac{\omega_0 - \omega_{n0}}{\omega_0} - \tilde{I}_n \int_0^{\bar{L}} d\bar{z}\, h(\bar{z}) \left\langle J'_s(k_{nt} r_L) \frac{u_t}{u_z} \sin\left[\Lambda + \tilde{\psi}_n - (m_n - m_\tau)\Theta_0 \right] \right\rangle_{\Lambda_0, \Theta_0} \tag{15}$$

where $\langle\ \rangle_{\Lambda_0,\Theta_0}$ denotes the average with respect to the initial momentum phases and guiding center angles of the electrons, and $\bar{L}$ is the normalized interaction length. The normalized current is given by:

$$\tilde{I}_n = \frac{|e|Z_0}{m_0 c^2 \bar{\omega}_0} \frac{J^2_{m_n - s}(k_{nt} R_0)}{\pi\left(1 - m_n^2 / x'^2_{m_n \ell_n}\right) J^2_{m_n}(x'_{m_n \ell_n}) \bar{W}} I_0 \tag{16}$$

where I_0 is the dc beam current, and the free–space impedance Z_0=377 ohms. The numerical calculations can be simplified by noting that the argument of the Bessel function $J_s(J'_s)$ which occurs in the equations of motion and the mode amplitude and phase source terms can be expressed as $k_{nt} r_L \approx s v_t / c$, and therefore these Bessel functions can be replaced by their small argument expansion with little loss of accuracy.

The time–dependent simulation is initiated by assigning a small initial amplitude and arbitrary phase to a set of modes which may participate in the interaction. The corresponding induced ac current density is obtained by integrating the equations of motion [Eqs. (5)–(7)] and is used to construct the source terms in Eqs. (15) and (16). Eqs. (15) and (16) can then be integrated for a single time step and the process repeated. The initial conditions for the equations of motion for a cold, phase–mixed electron beam are: $u_t(0) = u_{t0}$, $u_z(0) = u_{z0}$, a fixed guiding–center radius R_0; and $\Lambda(0) \equiv \Lambda_0$ and Θ_0 are uniformly distributed in the interval $[0, 2\pi]$. The density of azimuthal angles must be high enough that an adequate distribution over this interval is achieved for the quantity $(m_n - m_\tau)\Theta_0$ for all values of m_n. In the present case in which $|m_n|$ and $|m_{n0}|$ are ~ 40 and can have the same or opposite sign, it is necessary to include several hundred angles to preform this average accurately for all the interacting modes. The interaction efficiency is given by:

$$\eta = \frac{\gamma_0 - \left\langle \gamma(z = L, \Lambda_0, \Theta_0) \right\rangle_{\Lambda_0,\Theta_0}}{\gamma_0 - 1} \tag{17}$$

and the output power in the mode n is given by:

$$P_n(\tau) = \frac{\pi m_0^2 c^4}{2Z_0|e|^2} \frac{\left(1 - m_n / x'^2_{m_n \ell_n}\right) J^2_{m_n}(x'_{m_n \ell_n})}{Q_n J^2_{m_n \pm s}(k_{n\perp} R_0)} \overline{\omega}_0 \overline{W} |f_n(\tau)|^2 \tag{18}$$

for modes with $m_n = \pm|m_n|$, respectively.

For comparison with other work it is useful to introduce the following normalized parameters which are often used in gyrotron analysis (Danly and Temkin, 1986):

$$F_n = \frac{1}{\gamma_0 \beta_{t0}^{4-s}} \left(\frac{s^s}{2^{s-1} s!} \right) \frac{f_n}{x'_{m_n \ell_n}} \tag{19}$$

$$\mu = \pi \frac{\beta_{t0}^2}{\beta_{z0}} \frac{L}{\lambda} \tag{20}$$

$$\Delta = \frac{2}{\beta_{t0}^2} \left(1 - \frac{s \Omega_{z0}}{\omega_0 \gamma_0} \right) \tag{21}$$

where F_n is the normalized mode amplitude, μ is the normalized interaction length, and Δ is the mode detuning parameter.

III. Configuration Modeled

The gyrotron being modeled was inspired by a planned MIT 280 GHz gyrotron experiment. We were provided with a set of preliminary calculations for that device (Grimm 1991, Kreischer 1991), and used those values as the starting point for our work. The gyrotron is designed to operate in the $TE_{42,7}$–mode of a cylindrical cavity with wall radius R_w=1.25 cm, with the beam placed at a radius r_b=0.747 cm, in order to optimize coupling to the mode co–rotating with the electron beam (i.e., the $TE_{+42,7}$ mode, in our notation). Based on the work at MIT, the optimum magnetic field for this gyrotron was B_0=11.1 T. From a simulation for the realistic axial profile of the rf electric field, MIT derived a value L/λ=11.9, where L is the normalized interaction

length (full width at half maximum) in the cavity for an equivalent gaussian profile, and λ is the free–space wavelength of the radiation. The loaded cavity quality factor was Q=1180. The beam current was 50 A at a diode voltage of 90 kV. However, correcting for 6 kV of space charge depression of the beam voltage, the beam energy was 84 keV. The anticipated value of the beam α is 1.6, where $\alpha \equiv v_t/v_z$.

In general, the MIT values were the starting point of our study. However, the following alterations were made. First, while some simulation runs have been carried out at the indicated value of L/λ=11.9, the simulation runs reported in this paper were carried out at the slightly shorter value L/λ=8.26. Second, slightly larger magnetic fields (smaller detunings) were found necessary to produce stable oscillation either in the design mode, or in competing modes at approximately the same frequency, as discussed later in this paper. The most common value employed in the simulations was B_0=11.265 T.

IV. Results of the simulations

There were several separate issues to be resolved by these simulation studies, and a large parameter space to be investigated. In order to conserve simulation time, many of these issues were tackled separately, in limited simulation runs including only a small number of modes, a limited voltage ramp, or a limited number of simulation particles. During these shorter runs, the regime of stable operation in a particular final state was established, and the nature of the mode competition clarified. Finally, this led to a set of "long" simulations, which started at low voltage and attempted to model the entire sequence of modes, from the first that begins oscillating up to the final state.

Because of the cost of such long simulations, compromises were necessary with respect to the various simulation constants. An important limitation of this study was the various compromises required to keep the running time of the simulation

within available resources. There are a number of simulation constants whose scale size will affect the accuracy of the simulation. These include 1) the spatial mesh used to evaluate the interaction in the cavity, 2) the time step used to advance the fields, 3) the slope of the voltage ramp used to model start–up, 4) the number of particle phases included at each azimuthal location, and 5) the number of azimuthal beam positions (particles) included. During the shorter runs, an attempt was made to establish "experimentally" the minimum values of various simulation constants required to produce a simulation that was "qualitatively" in agreement with the result of simulations employing higher numbers of particles, more mesh points, etc. Based on a number of computational tests, these compromises should not affect the resulting final principal mode in the long simulations. However, the mode purity of the final state was separately addressed by using finer simulation constants in more limited simulation runs.

Additional limitations of this study include the use of a beam with no guiding center or α spread, and the (arbitrary) modeling of the beam current and α during the rise of the voltage pulse. The presence of guiding center spread would further complicate the mode competition, since additional series of modes would strongly couple to the beam, and the relative coupling of the various modes would change. Such spread could be included in the model in a straightforward way, by averaging the coupling coefficient for each mode over the radial spread—however, this was not done. The presence of α spread would slightly modify the growth rates of the various modes, and also have a small effect on the saturated efficiency. Including α spread would increase the particles required in each simulation by an order of magnitude. (In the experiment, it might also limit the maximum average α achievable.) This was not done. The current and α modeling are discussed in the next section.

IV.1 Results of the preliminary simulations

Before examining the simulation results, it is useful to examine calculations of the threshold for oscillation (starting current) for various modes. Starting current calculations were carried out using an analytic model that employs a sinusoidal approximation to the axial profile function of the mode. In order to match this to the gaussian model used by the time–dependent code, the length and cavity Q–factor were adjusted from the nominal values used in the time–dependent simulation to cause the minimum starting current, and its corresponding voltage, to agree with that for a gaussian profile for the $TE_{+42,7}$ mode. The starting current calculations were carried out for all first harmonic $TE_{m,\ell,1}$ modes with $|m| \leq 50$ and $\ell \leq 40$, where the third subscript "1" refers to the lowest order axial mode.

Starting current calculations as a function of voltage (beam kinetic energy) for B_0=11.265 T and a normalized radius r_b/R_w=0.6, corresponding to a beam radius r_b=0.747 cm, are shown in Fig. 1. In these calculations, the beam α is proportional to beam voltage, with α=1.6 at 84 keV, while the beam current is assumed to be 50 A, independent of voltage. Also, the Q of each mode is assumed to scale as the square of the mode frequency, with Q=1180 for the $TE_{42,7}$ mode. This modeling of current start–up is somewhat realistic, since the electron beam diode runs temperature rather than space–charge limited, and the current is known experimentally to turn on much more quickly than the voltage. The assumption that α is proportional to the beam kinetic energy is reasonable, given that the initial α in the diode is produced by the initial acceleration of the electrons by the electric field with a component normal to the magnetic field. However, no attempt has been made to model the current and beam α more realistically through such means as particle simulations. These same scaling laws were used in the time–dependent simulations.

For this $TE_{+42,7}$–mode design, the design mode has the lowest starting current (and highest growth rate) for a limited range of voltages in the vicinity of 70 keV. At

lower voltages, other $TE_{+m,7}$ and $TE_{-m,8}$ modes have the lowest starting currents (and highest growth rates). Based on a slow voltage risetime, the system should be expected to tune through a sequence of higher frequency modes before reaching conditions under which the $TE_{+42,7}$ mode can start oscillation. When the beam line enters the start oscillation curve for this mode, oscillation can build up provided that it is not suppressed by the rf electric fields of another mode. In a simple case, in which the only relevant modes were a sequence of $TE_{+m,7}$ modes, the $TE_{+42,7}$ mode would be expected to grow to saturation when the system detunes out of the $TE_{+43,7}$ mode. It is noteworthy that the 50 A beam current is greater than 10 times the starting current at 70 keV for the $TE_{+42,7}$ mode, and in fact exceeds the starting current for more than 15 other modes. However, the linear growth rate of each mode is inversely proportional to the starting current, so that for a system starting from noise at 70 keV, the $TE_{+42,7}$ mode should oscillate.

Accordingly, the first simulations employed just the $TE_{+42,7}$ mode, as in the MIT design, and determined its optimum detuning (i.e., magnetic field), and its final power and efficiency. The next simulations employed just the $TE_{+m,7}$ series of modes and determined the effect of mode competition and multimode effects. Mode competition limited the maximum detuning for the $TE_{+42,7}$ mode to the point at which the final state became the $TE_{+41,7}$, causing some reduction in efficiency, while multimode effects limited the purity of the final state, as significant $TE_{+41,7}$ and $TE_{+43,7}$–mode satellites appeared in the final $TE_{+42,7}$ state.

Each of the $TE_{\pm m,\ell}$ modes has a $TE_{\mp m,\ell}$ mode accompanying it at the same frequency, but with the opposite sense of rotation and, in general, a different coupling to the beam. The next issue to be examined was the effect of including the $TE_{-m,7}$ series of modes in the simulations. (This required a large increase in the number of simulation particles, as discussing in Section 2.) These oppositely rotating modes compete with the $TE_{+m,7}$ modes, but have a lower growth rate for the 0.747–cm beam

radius used in the simulations. It was found that the final state always consisted of modes with just one sense of rotation, as the stronger mode quickly suppressed the weaker one of opposite rotation. Thus, the mode competition between a $TE_{\pm m,\ell}$ mode and a $TE_{\mp m,\ell}$ mode does not lead to a multimode state (i.e., a standing mode). (In fact, prestarting the simulation with a large signal in the sense of rotation with the lower growth rate can lead to apparently stable oscillation whose sense of rotation is opposite to that which occurs due to ordinary start–up from noise.) However, during the mode hopping that occurs during the voltage ramp, short intervals of growth of the $TE_{-m,7}$ modes could be observed, before the corresponding (and faster growing) $TE_{+m,7}$ modes grew large enough to suppress them.

The only effect of keeping the $TE_{-m,7}$ modes in the simulations was an apparent slight reduction in the initial growth rate of the $TE_{+m,7}$ modes. In a situation involving strong competition between modes with almost identical growth rates and different values of m and ℓ, however, the presence of these $TE_{-m,7}$ modes can potentially affect the final state. Simulations including only the ℓ=7 series of modes, but with m=±40, ±41, ±42, ±43, ±44, have found a case with a magnetic field B_0=11.2375 T and a voltage ramp of 1.8 kV/ns, in which the system will skip from the $TE_{+43,7}$ to the $TE_{+41,7}$ due to the inclusion of oppositely rotating modes, while it ends up in the $TE_{+42,7}$ if only the plus modes are used in the simulation. This appears to be a risetime effect in the present case. However, it is easy to imagine cases with more closely spaced modes in which the $TE_{m-1,\ell}$ mode will be skipped over in favor of the $TE_{m-2,\ell}$ mode, even over very slow voltage ramps.

The next issue to be resolved was the affect of including $TE_{m,\ell}$ modes with $\ell \neq 7$. Based on Fig. 1, the most troubling modes were in the $TE_{-m,8}$ series. These modes in general occur at slightly higher frequencies than the nearest $TE_{+m,7}$ modes, but have comparable coupling to the electron beam at the design radius, and thus have a temporal advantage during the rise of the voltage pulse. In fact, for simulation runs

beginning at much lower voltages, this series of modes invariably suppressed the $TE_{+m,7}$ modes, even though the $TE_{+42,7}$ mode has the lowest start oscillation current in the vicinity of the final voltage. The reason for this will be discussed in this next section.

IV.2 Results of the long simulations

The culmination of a sequence of short runs to investigate parameter space and to understand the effect of varying the various simulation constants was the first long computer run (~9 hours of running time on a Cray X–MP) that attempted to model the entire time sequence during the voltage ramp, from start–up of the first mode, to the final state at full voltage (84 keV). This simulation is shown in Fig. 2. The beam radius was chosen to correspond to the MIT value (r_b/R_w=0.6) that optimizes coupling to the $TE_{42,7}$ mode, even though the result is operation in the $TE_{-39,8}$ mode. However, the magnetic field was chosen as B_0=11.265 T to produce stable oscillation in the $TE_{-39,8}$ mode at 84 keV. Based on an examination of Fig. 1, and the results of more limited simulation runs, only the $TE_{+m,7}$ and $TE_{-m,8}$ modes were included in this simulation, with the oppositely rotating modes in the ℓ=7 and ℓ=8 series excluded. A 60–ns voltage ramp was employed, beginning at 30 keV, followed by a 30–ns voltage flat–top at 84 keV. The simulation constants were chosen to minimize the length of the simulation without affecting the final results in a significant way. (However, the mode purity of the final state, and the final efficiency, were the subject of more limited runs with much finer simulation constants that confirmed the efficiency and multimode content of the final state.)

Figure 2 shows that the first mode to reach high power is the $TE_{-43,8}$ mode. (While Fig. 1 suggests that the $TE_{-44,8}$ mode should oscillate at ~26–28 keV, this was not seen in the preliminary simulations, and more accurate starting current calculations using the same gaussian profile used in the simulations, suggest that the

actual starting current for this mode is ≥ 50 A.) Shortly after the start of the $TE_{-43,8}$ mode, the $TE_{+46,7}$ mode begins to grow, but is quickly suppressed by the large amplitude $TE_{-43,8}$–mode oscillation. However, two satellite modes, the $TE_{-42,8}$ mode and the $TE_{-44,8}$ mode, grow up at about 10 ns. Subsequently, the $TE_{-43,8}$ mode is detuned by the voltage ramp, and begins to fall off. The higher frequency $TE_{-44,8}$ satellite mode also falls off. However, the lower frequency satellite, the $TE_{-42,8}$ mode, begins to grow, saturates at ~16 ns, and remains at high power till ~24 ns. During this period, the previous oscillating mode, the $TE_{-43,8}$ mode, has become a satellite mode, and a new satellite, the $TE_{-41,8}$ mode, has appeared. This mode progression continues through the voltage ramp until the final $TE_{-39,8}$ mode oscillates. Its satellites are the $TE_{-40,8}$ mode and the $TE_{-38,8}$ mode. Figure 3 shows the overall multimode efficiency during the mode sequence.

Figure 2 shows mode evolution within the family of $TE_{-m,8}$ modes, with no serious competition from the $TE_{+m,7}$ modes. Each of the intermediate states, from the first mode to start oscillation, the $TE_{-43,8}$ mode, to the final $TE_{-39,8}$ mode, is a multimode state, with its $m'=m\pm1$ mode satellites present at levels >1%. However, close examination of the simulation shows that active mode competition takes place only during each transition from a particular $TE_{-m,8}$ mode to the lower frequency $TE_{-m+1,8}$ mode. This competition involves both $TE_{-m,8}$ modes and $TE_{+m,7}$ modes. This can be seen in Fig. 4, which shows only the $TE_{+m,7}$ modes from the simulation. With the exception of the $TE_{+46,7}$ mode, the remaining $TE_{+m,7}$ modes show growth spurts only during the transition between oscillation in adjacent $TE_{-m,8}$ modes. They are turned loose to grow as each $TE_{-m,8}$ mode detunes out of its high power oscillation, but are quickly suppressed as the next $TE_{-m+1,8}$ mode grows from a satellite mode to high power oscillation. In the final state, the power in the main $TE_{-39,8}$ mode is ~1.2 MW, while the $TE_{-40,8}$ satellite is at 45 kW and the $TE_{-38,8}$ satellite is at 30 kW. Thus, the overall mode purity is about 94%.

Figure 5 shows the result of an identical simulation employing only the $TE_{+m,7}$ modes. As expected, the system proceeds in a sequence of $TE_{+m,7}$ modes, and the final state is the $TE_{+42,7}$ mode, with $TE_{+41,7}$ and $TE_{+43,7}$ satellite modes.

5. Discussion of the results

It was found that for systems of the order of length of the proposed MIT design (or somewhat shorter), the final state (i.e., during the voltage flat–top) was a multimode state, with the $m\pm1$ satellites of the oscillating $TE_{m,\ell}$ mode present at the ~2–5% power level. This has some consequence with respect to the utility of the final state for particular applications. In addition, the intermediate states during the start–up voltage ramp were multimode states, an effect that plays a strong role in determining the particular mode which will dominate the final state. The multimode complexion of these oscillating states seems to be a function of the mode density. To test this hypothesis, a simulation run was carried out employing only alternate $TE_{-m,8}$ modes. In this case, the satellite modes have twice the frequency separation. The maximum satellite level seen was <0.1%.

Mode competition is critical during the voltage risetime. Generally speaking, due to the presence of a voltage ramp at the leading edge of the voltage pulse, the operating mode is not the *first* mode to reach high power, but the *last* mode to reach high power, during the voltage ramp. More specifically, the system passes through a sequence of high power modes. (In the simulations, these intermediate modes last only ~10 ns. However, in the much slower experimental voltage ramp, each mode might last hundreds of ns.) The same type of mode sequence was invariably observed during the voltage ramp, as follows. The first mode to start oscillation simply started a sequence of ~5 high power modes, at progressively lower frequency, as each mode was detuned with increasing voltage, leading to the final mode. (Final here must be qualified by noting that we have modeled only a few tens of nanoseconds of the

voltage flat–top, and the apparent stability during this time interval may not persist for the microseconds of the experimental voltage pulse.) We have found that each intermediate state is a multimode state, since when a $TE_{m,\ell}$ mode is large, it will have satellites at $TE_{m\pm1,\ell}$. This is a result of a "well–understood" process (Levush and Antonsen 1990) whereby the $TE_{m\pm1,\ell}$ modes grow up due to a resonance condition involving $2\omega_{m,\ell}-\omega_{m+1,\ell}-\omega_{m-1,\ell}\approx0$. However, $TE_{m',\ell'}$ modes in other radial series $\ell'\neq\ell$, with $m'\neq m\pm1$, do not become satellites, and in fact are found in the simulations to be strongly suppressed. Since the satellite modes are from the same set of radial modes (e.g., $TE_{+m,7}$ or $TE_{-m,8}$ modes), the lower frequency $TE_{\pm m\mp1,\ell}$ satellite mode will have both gain and higher initial amplitude than other competing modes, just as the $TE_{\pm m,\ell}$ mode detunes out of its nonlinear operation due to the effect of the positive voltage ramp.

In fact, the simulations indicate the situation is still more strongly biased in favor of the lower frequency satellite mode. That is, the $TE_{\pm m\mp1,\ell}$ mode, which begins at $\geq 1\%$ of the power of the main mode (or $\geq 10\%$ of its rf electric field), will begin to grow and ultimately to suppress the $TE_{\pm m,\ell}$ mode, due to the voltage ramp, so that the $TE_{\pm m,\ell}$ mode actually turns off at a slightly lower voltage than it would in a single mode run. Thus, no other modes have much likelihood of taking over, and there is a strong tendency for the system to evolve in a sequence of modes with constant radial index (and constant sense of rotation), even if it would appear that at full voltage, this set of modes does not have the lowest threshold current (highest growth rate).

There is a window in time during which the dominant mode has begun to fall off, and the lower frequency satellite mode to grow, during which other modes can also compete. However, it is a very limited window. That is, while the satellite is growing by only ~100× in power to saturation (and only ~30× to the point at which nonlinear suppression of other modes begins), another mode would have to come out of the noise level (which was arbitrarily set at 1 kV/cm at the beam for each mode), and

grow large enough to suppress the satellite mode. Since this competition is based on relative growth rates, rather than the voltage risetime, it is not necessary to simulate a ramp as slow as the experimental ramp (several microsecond risetime) to adequately model this aspect of mode competition.

Therefore, to design for operation in the $TE_{+42,7}$ mode, for instance, it is not sufficient to ensure that this mode has the lowest starting current in the vicinity of the final voltage. In practice, at the beam radius chosen to optimize the coupling to the $TE_{+42,7}$ mode, the $TE_{-m,8}$ modes *always* start first, and thus the final state is instead the $TE_{-39,8}$, even though this mode has a higher starting current in the vicinity of the design voltage. Instead, one must ensure that a higher frequency $TE_{+m,7}$ mode, such as the $TE_{+45,7}$ mode, is the first mode to start oscillation during the rise of the voltage ramp.

To test this supposition, a search was made for a beam radius at which a $TE_{+m,7}$ mode would oscillate first. Figure 6 shows the starting current as a function of voltage for the case of B_0=11.265 T and r_b/R_w=0.624, corresponding to a beam radius of 0.780 cm. In this case, the $TE_{+47,7}$ mode should be the first mode to oscillate, followed by the $TE_{+46,7}$. (However, there is a small interval near 32 keV where the $TE_{-43,8}$ mode has the lowest starting current.) Figure 7 shows the results of a time–dependent simulation run for this beam radius. (The remaining parameters are as in Fig. 2.) As expected, the $TE_{+m,7}$–mode series dominates in a sequence beginning with the $TE_{47,7}$ mode and ending with the $TE_{+42,7}$ mode. The $TE_{-43,8}$ mode shows some growth at ~10 ns, but is quickly suppressed by the $TE_{+46,7}$ mode. This simulation run included the $TE_{-m,7}$ modes as well, since the $TE_{-42,7}$ mode actually has a lower starting current than the $TE_{+42,7}$ mode. However, the progression is a series of $TE_{+m,7}$ modes, as predicted from the previous long simulation, and, despite its higher linear growth rate, the $TE_{-42,7}$ mode is completely suppressed in the final state, because the $TE_{+42,7}$ mode was already present at a significant level as the

system detuned with voltage from the $TE_{+43,7}$ mode. The saturated state again appears to be a multimode state, with substantial amounts of the $TE_{+43,7}$ and $TE_{+41,7}$ modes present.

6. Summary

We have carried out a simulation study of mode competition in highly overmoded gyrotron oscillators. The parameters of our simulation were chosen in light of a 280 GHz, 1 MW gyrotron design from MIT. The study addressed the difficulty of causing the system to oscillate in the design mode in the presence of competition from other modes, and demonstrated the difficulty of achieving stable single–mode operation. While the simulations were computationally intensive, and could not pursue all issues relevant to long pulse operation, they were used to study numerous separate cases, and established trends with respect to the problems of mode competition during the start of the voltage pulse. They also addressed the mode purity of the final state. Specifically, it was found that because of multimode coupling, the system had a very strong tendency to remain in a particular series of $TE_{m,\ell}$ modes, with m of a particular sign, and ℓ constant, during the voltage ramp. Thus, controlling the first mode to oscillate can permit control of the final mode to oscillate, even in the presence of substantial competition from modes with different values of ℓ. The efficiency of the final state depends strongly on the final detuning (as well as on the presence of parasitic modes). In general, the optimum detuning derived for a single mode was unachievable due to mode competition. Finally, for systems of the length of the MIT design (or somewhat shorter), the final state appears to be a multimode state, with the $TE_{m\pm1,n}$ modes present at approximately the 3–5% level. This will degrade the useful efficiency of the gyrotron for many applications. In addition, the efficiency is somewhat degraded because the magnetic field detuning that optimizes efficiency in a single mode run, will not generally result in operating in the same mode in the presence of mode competition.

ACKNOWLEDGMENTS

We acknowledge useful discussions with W.M. Manheimer. This work was supported in part by the U. S. Office of Naval Research and in part by the Office of Fusion Energy of the U. S. Department of Energy. The Cray computer time was provided by an NRL 6.1 Cray X-MP Production Time Grant.

References

ANTONSEN, T., LEVUSH, B., and MANHEIMER, W. M., 1990, Stable single mode operation of a quasioptical gyrotron. *Physics of Fluids B*, **2**, 419–426.

BONDESON, A., MANHEIMER, W. M., and OTT, E., 1983, "Multimode analysis of quasi–optical gyrotrons and gyroklystrons" in *Infrared and Millimeter Waves*, edited by Button, K.J. (Orlando: Academic Press), vol. 9, chap. 7, pp. 309–339.

BORIE, E. and JÖDICKE, B., 1988, Comments on the linear theory of the gyrotron. *IEEE Transactions on Plasma Science*, **16**, 116–121.

DANLY, B. G., and TEMKIN, R. J., 1986, Generalized nonlinear harmonic gyrotron theory. *Physics of Fluids*, **29**, 561–567.

DUMBRAJS, O., NUSINOVICH, G. S., and PAVELYEV, A. B., 1988, Mode competition in a gyrotron with tapered external magnetic field. *International Journal of Electronics*, **64**, 137–145.

FLIFLET, A. W., READ, M. E., CHU, K. R., and SEELEY, R., 1982, A self–consistent field theory for gyrotron oscillators: application to a low Q gyromonotron. *International Journal of Electronics*, **53**, 505–522.

FLIFLET, A. W., 1986, Linear and nonlinear theory of the Doppler–shifted cyclotron resonance maser based on TE and TM waveguide modes. *International Journal of Electronics*, **61**, 1049–1080.

FLIFLET, A. W., LEE, R. C., GOLD, S. H., MANHEIMER, W. M., and OTT, E., 1991, Time–dependent multimode simulation of gyrotron oscillators. *Physical Review A*, in press.

GRIMM, T., 1991, private communications.

KREISCHER, K., 1991, private communications.

LAMB, W. E., JR., 1964, Theory of an optical maser. *Physical Review*, **134**, A1429–A1450.

LEVUSH, B., and ANTONSEN, T.M., JR., 1990, Mode competition and control in high–power gyrotron oscillators. *IEEE Transactions on Plasma Science*, **18**, 260–272.

LIN, A. T., LIN, C.–C., YANG, Z. H., CHU, K. R., FLIFLET, A. W., and GOLD, S.H., 1988, Simulation of transient behavior in a pulse–line–driven gyrotron oscillator. *IEEE Transactions on Plasma Science*, **16**, 135 –141.

MOISEEV, M. A., and NUSINOVICH, G. S., 1974, Concerning the theory of multimode oscillation in a gyromonotron. *Izvestia Vysshikh Uchebnykh Zavedenni, Radiofizika*, **17**, 1709 (*Radiophys. Quantum Electron.*, **17**, 1305).

NUSINOVICH, G. S., 1981, Mode interaction in gyrotrons. *International Journal of Electronics*, **51**, 457–474.

SARGENT, M., III, SCULLY, M. O., and LAMB, W.E., Jr., 1974, *Laser Physics* (Reading, Mass.: Addison–Wesley), chap. 8.

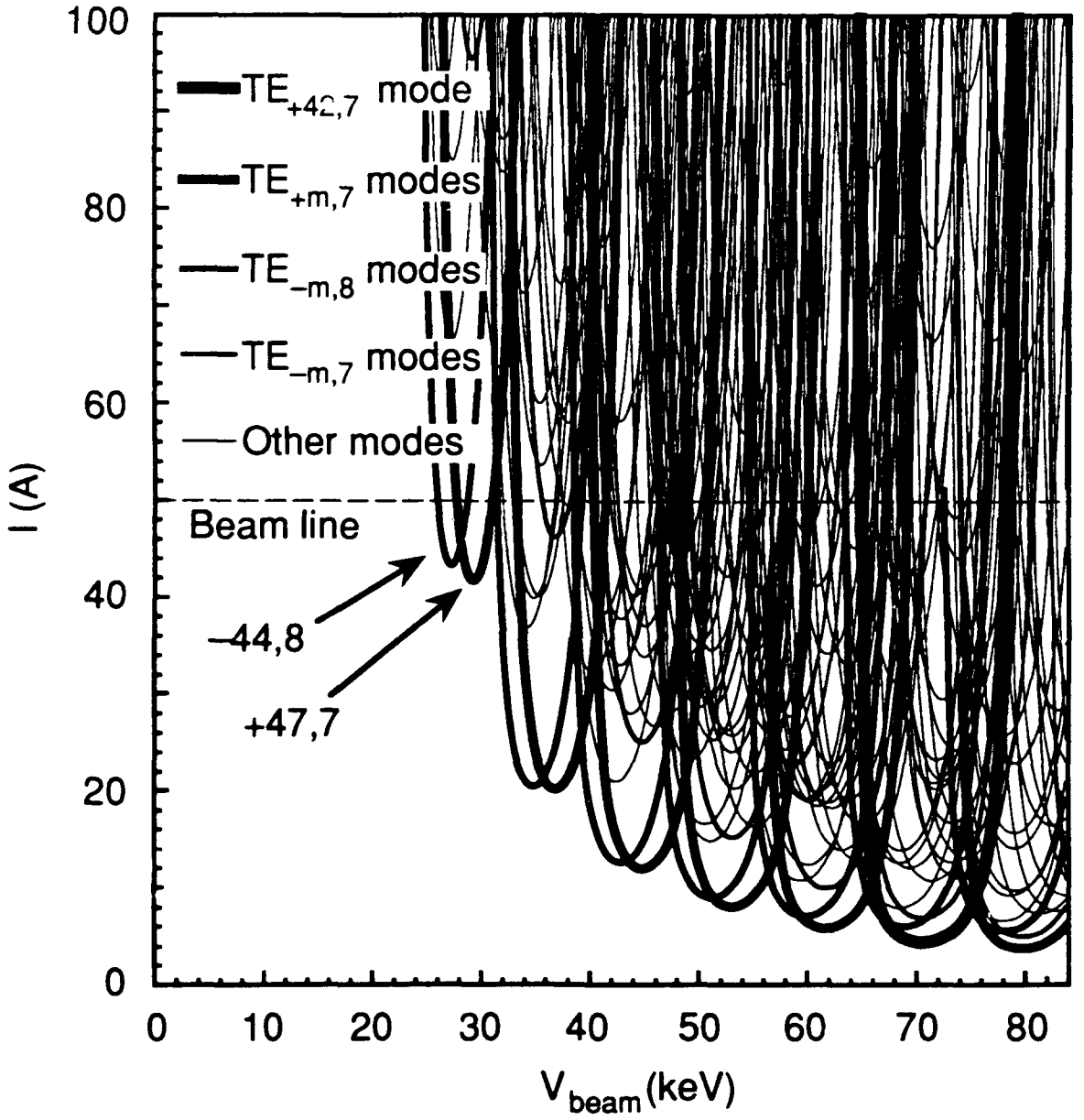

Figure 1. Start current calculations for the MIT gyrotron design (but with L/λ=8.26), for B_0=11.265 T, r_b/R_w=0.6.

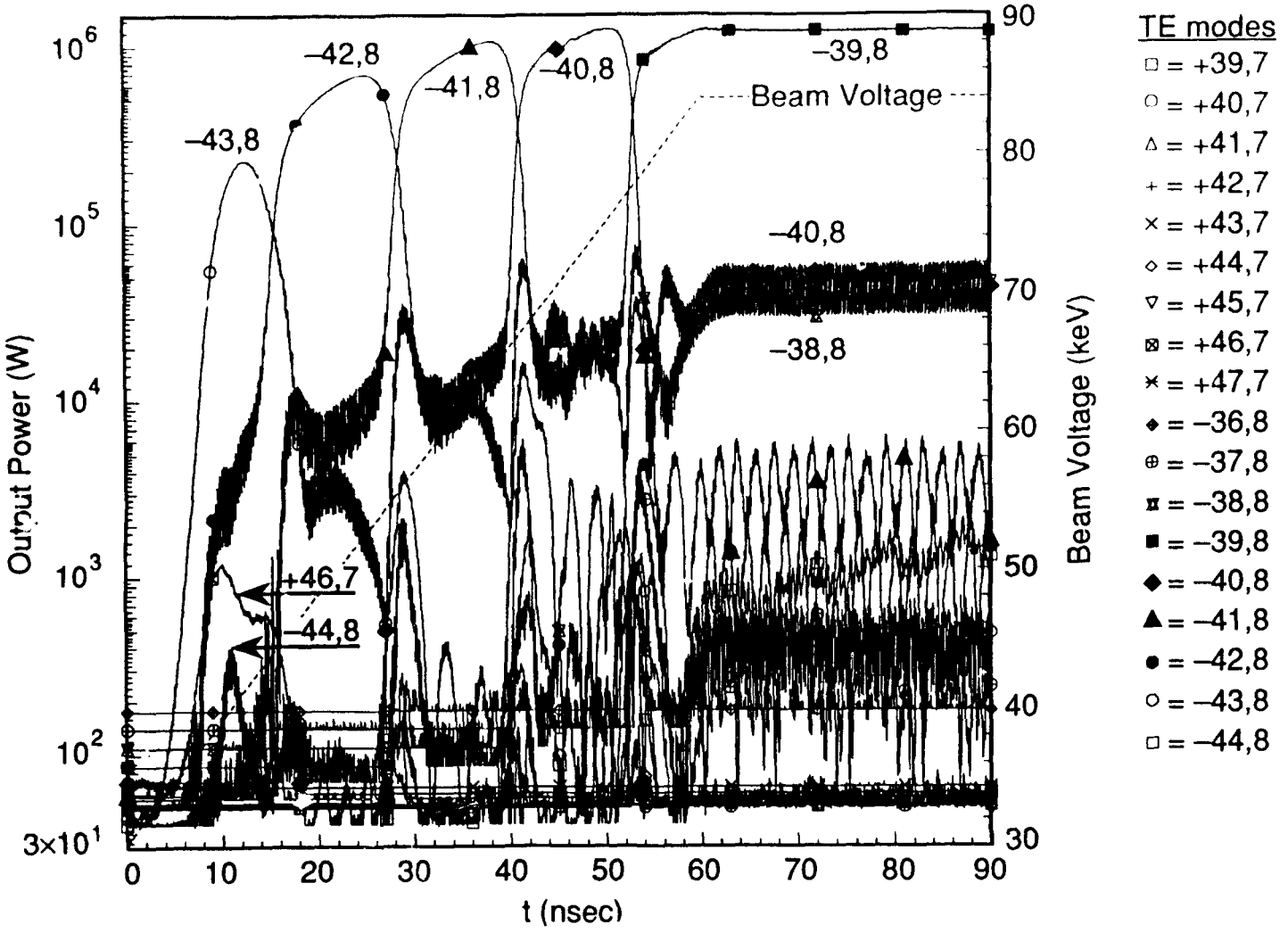

Figure 2. Time–dependent multimode simulation of gyrotron power during start–up with a voltage ramp, for B_0=11.265 T, r_b/R_w=0.6. $TE_{+m,7}$ modes and $TE_{-m,8}$ modes are included in the simulation.

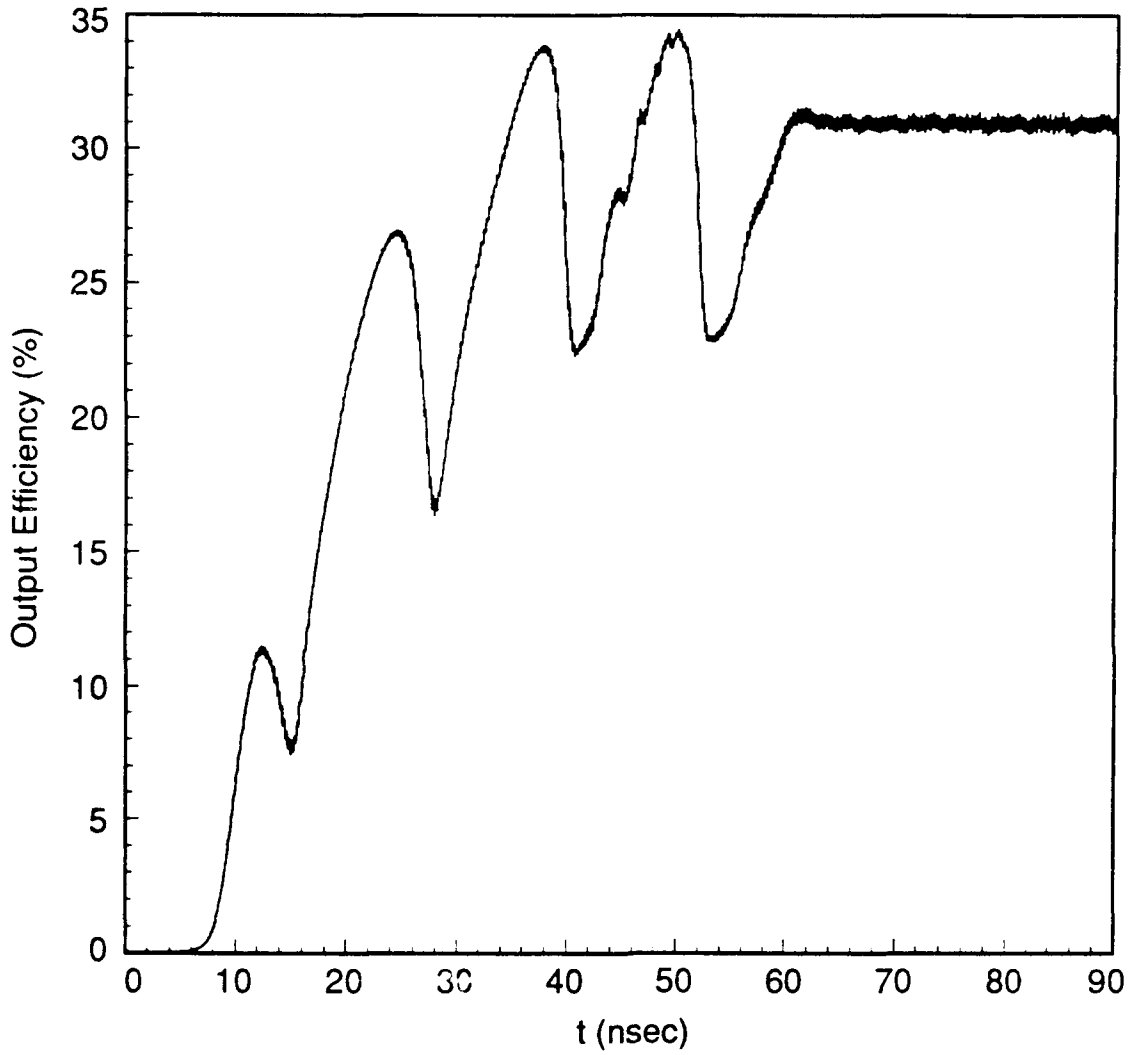

Figure 3. Efficiency from the simulation.

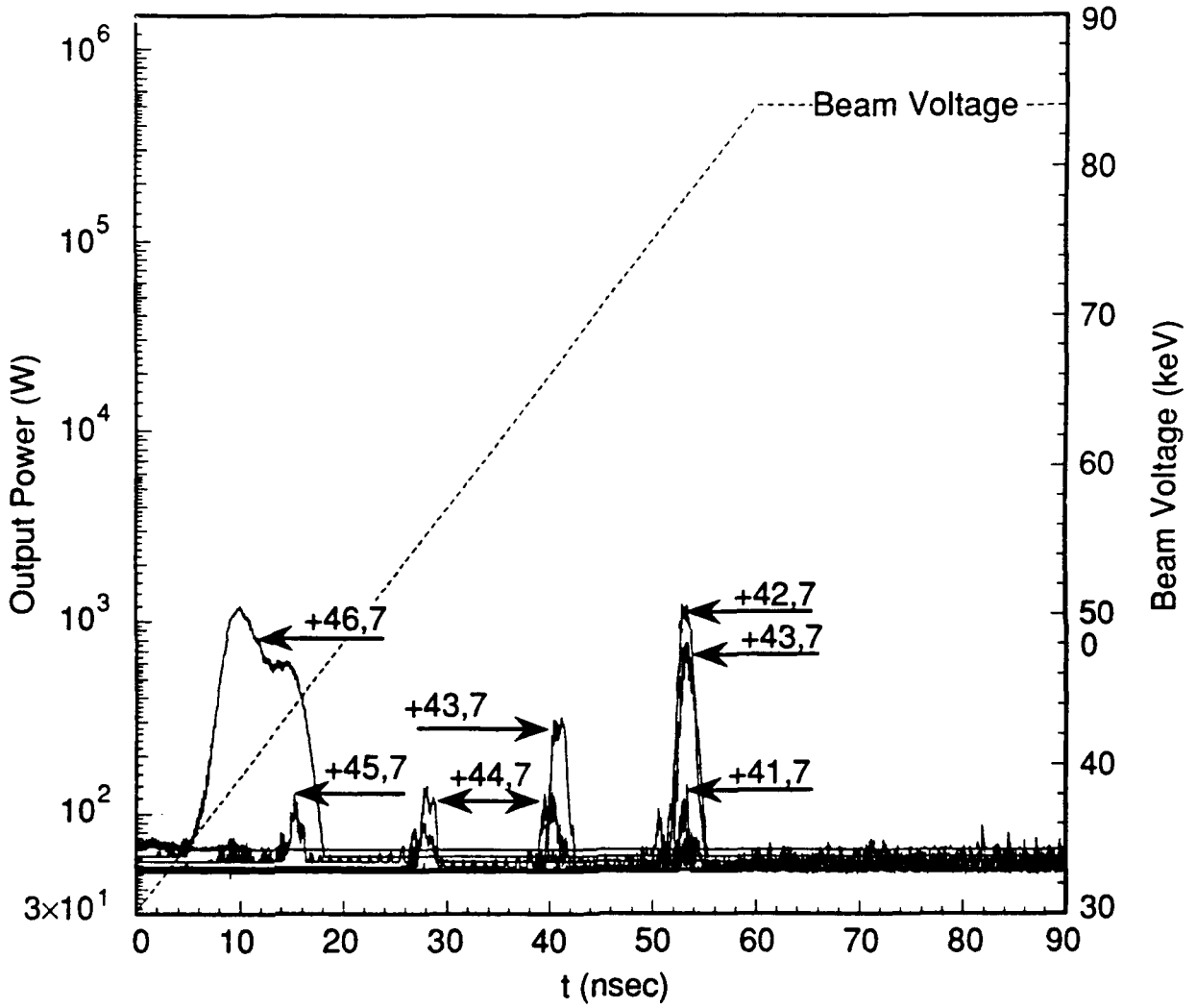

Figure 4. Plot of only the $TE_{+m,7}$ modes from the simulation.

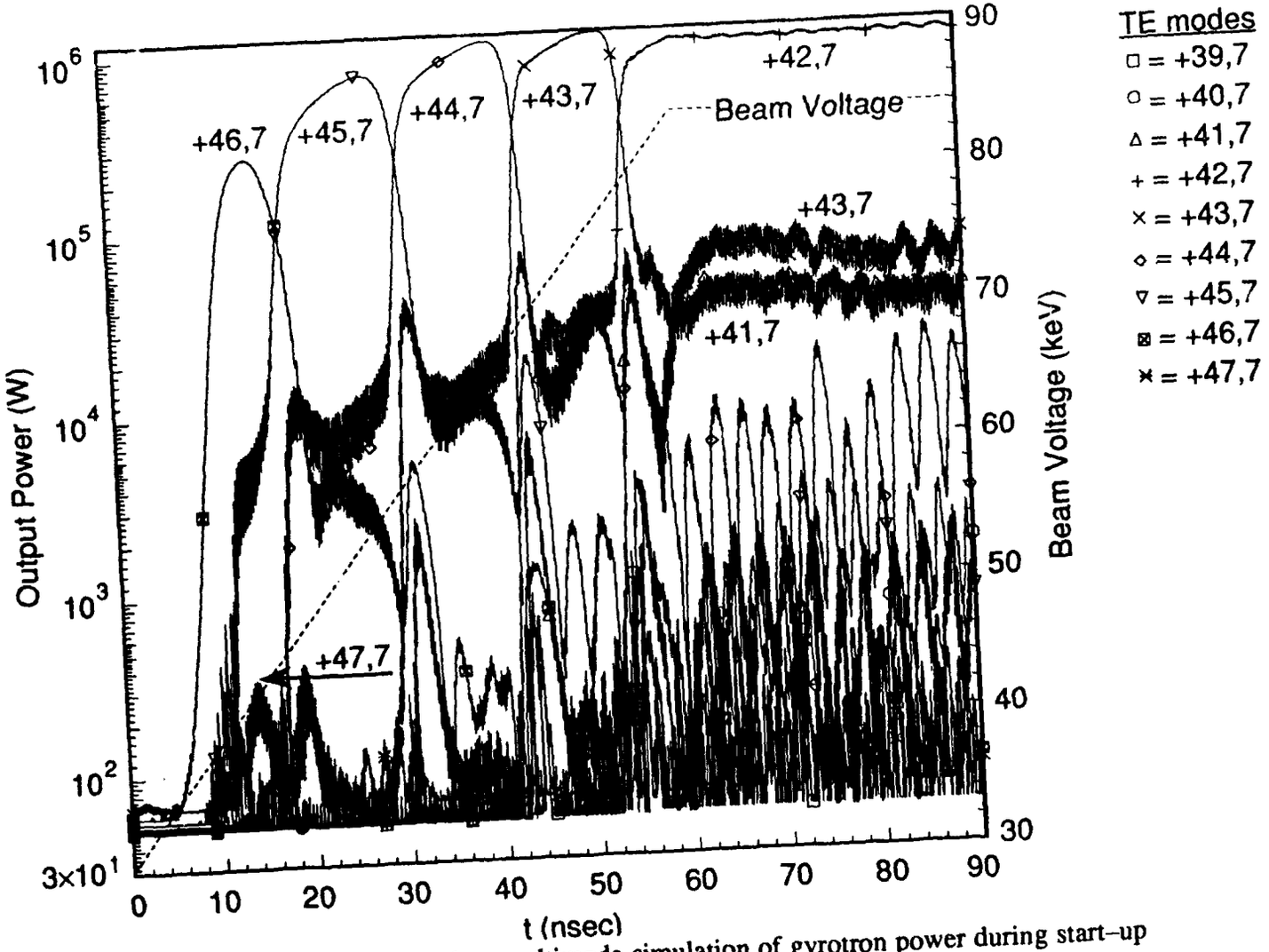

Figure 5. Time–dependent multimode simulation of gyrotron power during start–up with a voltage ramp, for B_0=11.265 T, r_b/R_w=0.6, employing only the $TE_{+m,7}$ modes.

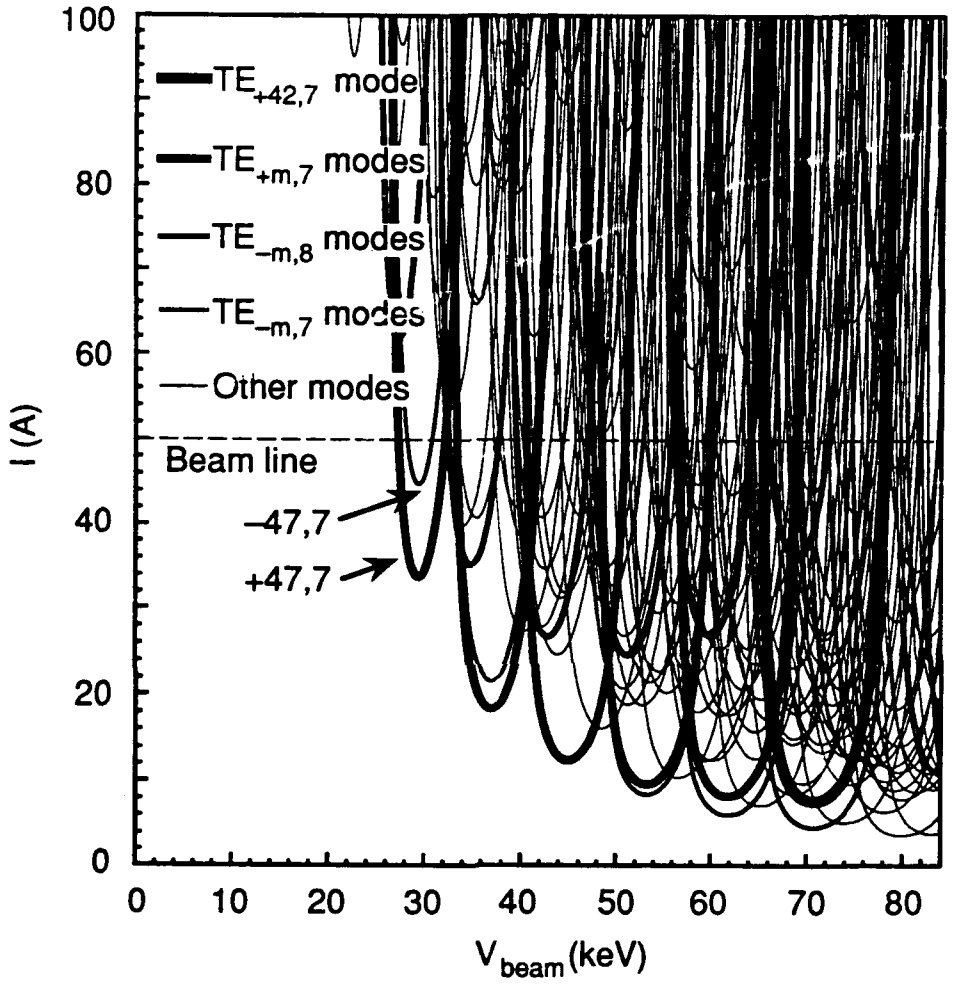

Figure 6. Start current calculations for B_0=11.265 T, r_b/R_w=0.624.

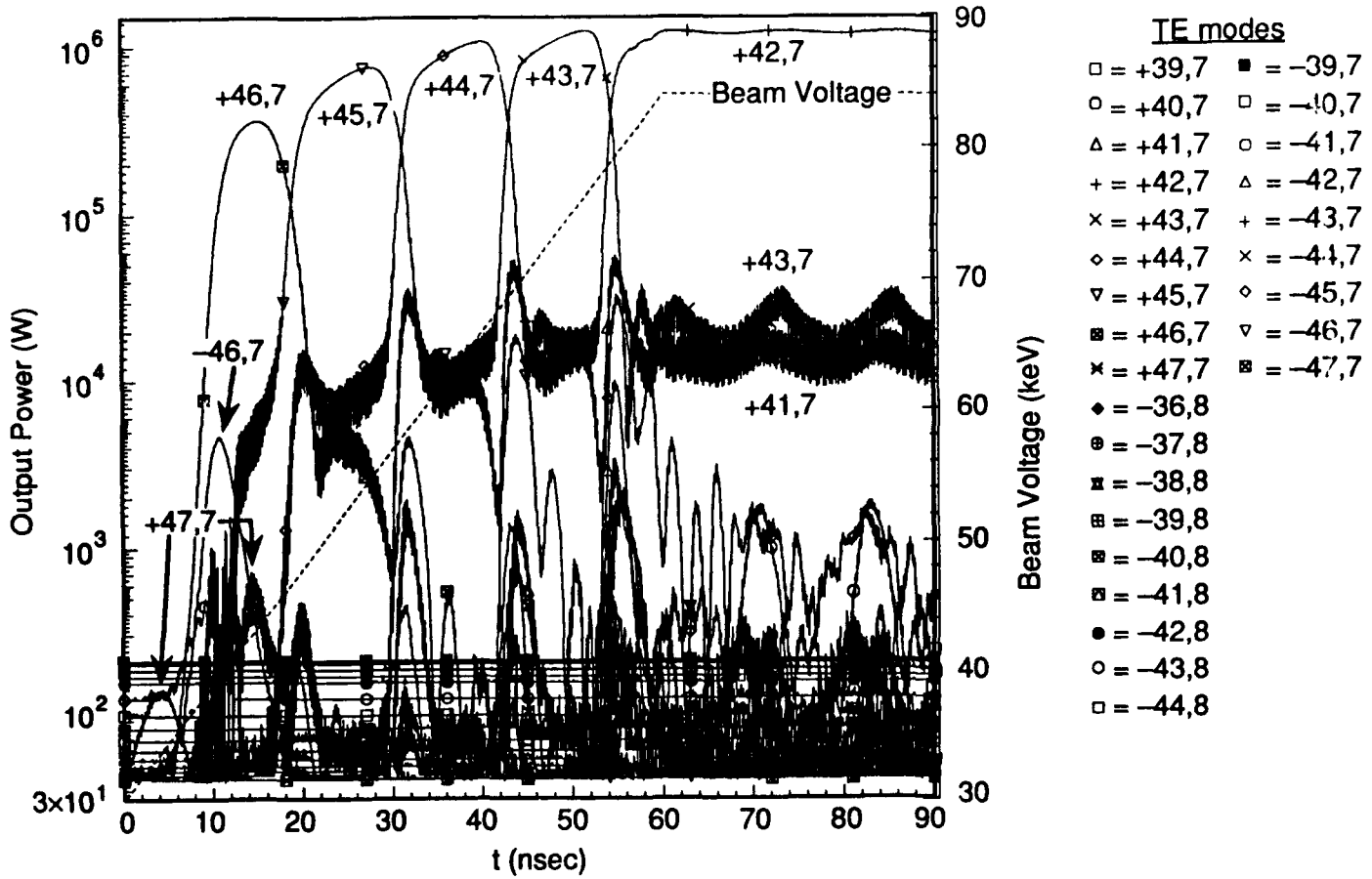

Figure 7. Time–dependent multimode simulation of gyrotron power during start–up with a voltage ramp, for B_0=11.265 T, r_b/R_w=0.624. $TE_{\pm m,7}$ modes and $TE_{-m,8}$ modes are included in the simulation.